Chapter 7: Instrument Calibration Using Tandem Differential Mobility Analysis with a Microplasma Source

"Measure what is measurable, and make measurable what is not so." — Galileo Galilei

7.1. Introduction

Measurements of ambient aerosols have demonstrated the abundance of nanoparticles in the atmosphere.[1] Small particles accumulate to a critical concentration and begin to agglomerate, forming larger particles with a broad distribution of sizes.[2] The particle size and concentration are important factors in determining the aerosol dynamics.[3]

The primary instrument to measure particle size distributions is the differential mobility analyzer (DMA). The device classifies particles based on small differences in mobility (Z_P) of charged particles between two electrodes with a fixed spacing (b) in an electric field ($E = V/b$). A particle-laden stream (Q_a) enters the classifying region through one electrode where it is combined with a laminar sheath flow (Q_{sh}). The electric field forces the particles through the particle-free sheath flow toward the other electrode. After a fixed distance (l), the flow is divided unequally with a portion exiting (Q_s; i.e., the sample flow) the electrode opposite of the aerosol entrance. This stream is directed to a particle counting device to measure concentration. The remaining flow is exhausted as the excess flow (Q_{ex}).

The applied voltage for a given device determines the mean mobility (Z_p^*) of the transmitted particles. Particles with a lower mobility than the mean will be removed with the excess flow whereas particles with a higher mobility will be deposited onto the electrode. This implies that a range of particle mobilities will be transmitted around the mean mobility selected.

The performance of the DMA is measured with two parameters: transmission efficiency (η) and resolution (R). Transmission efficiency is defined as the fraction of charged particles entering the device with a fixed mobility that emerge through the sample outlet with the appropriate voltage applied. A transmission lower than unity is caused by particle losses in the different regions of the device. Resolution is defined as

$$R = \frac{Z_p^*}{\Delta Z_{FWHM}}, \tag{7.1}$$

where ΔZ_{FWHM} is the full width at half maximum of the distribution. The theoretical maximum resolution is Q_{sh} / Q_a, but particle diffusion and axial asymmetry in the sizing region decrease the measureable resolution. Forehand knowledge of resolution and transmission allows data correction, enabling a more accurate assessment of aerosol particle size distribution.

A new DMA was recently reported that could measure particles in the 1 to 12.5 nm size range.[4] The instrument resolution for the mobility diameter range of 1 to 2 nm through electrospray of molecular ions, as reported previously. The instrument achieved considerable resolution over this range, but additional calibration data is needed to determine the transmission and the resolution of the device for the remainder of the size range.

A standard method to calibrate a DMA involves using two instruments in series in a configuration known as the Tandem DMA (TDMA).[5] A source produces particles that are passed to the first DMA. The first DMA is operated with a constant applied voltage, passing a narrow mobility distribution of particles to either a particle counter or a second DMA. The particle counter records the particle concentration (N_1) upstream of the second DMA before directing the flow through the second DMA. The second DMA is operated in voltage stepping mode, collecting a particle size distribution that reflects the combined resolutions of the two devices. As particle concentration (N_1) is not measured during the voltage scans of the second DMA, the source must be capable of producing a stable concentration of a fixed size distribution.

Calibration using the TDMA arrangement is difficult in the 2 to 4 nm size range due to the lack of a stable source. Electrospray of molecular ions have been successfully employed below 2 nm to determine instrument resolution,[6] but becomes more difficult above 2 nm as the particles will tend to attain multiple charges. A source aerosolizing polystyrene beads work well above 10 nm, but a well-characterized sample is not currently available below 5 nm. In this section, a recently developed aerosol synthesis technique based on a microplasma is examined as a possible source. It has been demonstrated the microplasma can operate stably for extended periods of time and produce a high concentration of particles in the 1 to 5 nm size range, and therefore should be suitable as a particle source.

7.2. Experimental Method

The microplasma source was combined with two nano-RDMAs in the TDMA arrangement, as shown in figure 7.1. The operation of a single microplasma has been

discussed previously.[7] Briefly, this system consisted of a stainless steel capillary (I. D. ≈ 180 μm) and a stainless steel tube (O. D. ≈ 3 mm) between which the microplasma is maintained. Through the capillary, a stream is passed that contains an ultrahigh purity (UHP) argon stream and a silane (50 parts per million (ppm)) in argon mixture stream at a combined flow rate of 150 standard cubic centimeters per minute (sccm), as controlled with two mass flow controllers (MFCs). The electrode assembly is sealed inside a glass tube (O. D. ≈ 12 mm) using standard Swagelok and UltraTorr fittings. A third MFC flows a sheath gas of UHP argon at 450 sccm that is combined with the first stream in the afterglow portion of the microplasma. This combined flow (total of 600 sccm) is introduced into the aerosol inlet of the nano-RDMA.

As the particle size produced from the microplasma is sensitive to pressure variations, the flows in the system must be precisely matched. This means that the sheath (Q_{sh}) and excess (Q_{ex}) flow rates of each nano-RDMA are precisely matched using a Gillibrator. The aerosol inlet (Q_a) and sample flow (Q_s) rates are matched as well. Matching the inlet and sampling flow rate is accomplished using a leak valve backed with a diaphragm pump, permitting flow rate matching to within ±1 sccm.

All particle size scans were made in the voltage stepping mode. This process involved setting the voltage across the DMA electrodes and measuring the current produced from the charged particles that were transmitted through the DMA. The current was measured with a home-built Faraday cup electrometer sensitive to ±1 fA. To establish steady-state current, the voltage was set followed by a two second delay before the current was measured for one second. Rather than using a single electrometer, two

matched electrometers were used to minimize transmission lines and to allow fast switching between the first and second nano-RDMA.

A computer was used to scan the voltage applied to the first device and to record the current measured with the first electrometer. After three consecutive measurements, the size-selected particle-laden flow was directed toward the second nano-RDMA. A fixed voltage was applied to the first nano-RDMA while the computer scanned the voltage applied to the second nano-RDMA while the current measured with the second electrometer was recorded. The voltage on first device was systematically varied to cover the broadest range of voltages that could be spanned while maintaining adequate particle concentration delivered to the second electrometer. After scanning through the voltage range, the flow was re-directed to the first electrometer and the scans were recorded, allowing comparison of the size distributions before and after. If the before and after distributions did not agree, the sequence was repeated. Generally, the before and after distributions agreed except if size distributions were collected shortly after the microplasma was first struck. If the microplasma was allowed to equilibrate for 30 minutes after striking the microplasma, the size distributions were quite stable. This procedure was repeated for four different silane concentrations (i.e., 1, 2, 3, and 4 ppm). Changing the precursor concentration allowed probing of different voltage ranges with some overlap as well as different size distribution polydispersities.

The measured size distributions were analyzed to determine resolution and transmission. First, the concentration data were normalized (N_2/N_1) and plotted against the normalized mobility (Z_2/Z_1). The resulting data were analyzed using the MatLab function *nlinfit*.

7.3. Results and Discussion

The first calibration experiments used nano-RDMA 2 in the first position and nano-RDMA 1 in the second position. The mobility distribution was measured with the first nano-RDMA, as shown in figure 7.2. The mobility distribution before and after analysis with the second nano-RDMA agreed well with one another, and the measured distribution could be fit with a lognormal distribution.[8] The parameters of the lognormal fits are listed in table 7.1. The mean inverse mobility increased (i.e., size increased) and the distribution broadened with increasing silane concentration, as described previously (chapter 4).

These parameters are not the actual characteristics of the mobility distribution produced with the microplasma. The data represents the convolution of the mobility distribution (f_{LN}) with the Stolzenburg transfer function of the nano-RDMA (Ω_{Stolz}):

$$N_1(Z_P) = \eta_1 f_{LN}(1/Z_P^*, N, 1/Z_{Pg}, \sigma_g) * \Omega_{Stolz,1}(Z_P, Z_p^*, \sigma_{Stolz}, \beta, \delta_{FR}), \qquad (7.2)$$

where η_1 is the transmission efficiency, Z_p^* is the convolution variable, N is the concentration, Z_{Pg} is the geometric mean mobility, σ_g is the geometric standard deviation, Z_P is the mobility, σ_{Stolz} is the Stolzenburg broadening coefficient of the distribution, δ_{FR} is a parameter used to correct for unbalanced flows (δ_{FR} = 0 in this report), and β is the ratio of aerosol to sheath flow (Q_a / Q_{sh}) when δ_{FR} = 0. The lognormal distribution is defined as

$$f_{LN}(1/Z_P^*, N, 1/Z_{Pg}, \sigma_g) = \frac{dN}{d\ln Z_P^*} = \frac{N}{(2\pi)^{1/2}\ln\sigma_g}\exp\left(-\frac{1}{2}\left(\frac{\ln\left(\frac{1/Z_P^*}{1/Z_{Pg}}\right)}{\ln\sigma_g}\right)^2\right), \qquad (7.3)$$

and the transfer function is defined as

$$\Omega_{Stolz}(Z_P, Z_p^*, \sigma_{Stolz}, \beta, \delta_{FR}) = \frac{\sigma_{Stolz}}{\sqrt{2}\beta(1-\delta_{FR})}\left[\begin{array}{l}\varepsilon\left(\frac{Z_p^*/Z_P-(1+\beta)}{\sqrt{2}\sigma_{Stolz}}\right)+\varepsilon\left(\frac{Z_p^*/Z_P-(1-\beta)}{\sqrt{2}\sigma_{Stolz}}\right)\\ -\varepsilon\left(\frac{Z_p^*/Z_P-(1+\beta\delta_{FR})}{\sqrt{2}\sigma_{Stolz}}\right)-\varepsilon\left(\frac{Z_p^*/Z_P-(1-\beta\delta_{FR})}{\sqrt{2}\sigma_{Stolz}}\right)\end{array}\right], \qquad (7.4)$$

where

$$\varepsilon(x) = x \cdot erf(x) + e^{-x^2}/\sqrt{\pi}\,, \qquad (7.5)$$

where *erf(x)* is the error function. The Stolzenburg transfer function can be modeled as a lognormal distribution when σ_{Stolz} is not too small:

$$f_{DMA}(Z_P^*, 1, Z_P, \sigma_{g,DMA}) = \frac{1}{(2\pi)^{1/2}\ln\sigma_{g,DMA}}\exp\left(-\frac{1}{2}\left(\frac{\ln(Z_P^*/Z_P)}{\ln\sigma_{g,DMA}}\right)^2\right), \qquad (7.6)$$

where $\sigma_{g,DMA}$ is the geometric standard deviation of the distribution. The value of $\sigma_{g,DMA}$ is not the value of σ_{Stolz}.

The analysis to this point is similar to that presented previously.[*9-10*] One assumption made in this analysis was that the particle distribution was sufficiently broad that the concentration does not change appreciably over the width of Ω_{Stolz}. The microplasma produces a narrow size distribution that may not be sufficiently broad to justify this assumption. The assumption is not necessary provided that σ_{Stolz} is not small. The solution to the convolution for a single modal distribution takes the form:

$$N_1(Z_P) = \int_0^\infty f_{LN}(1/Z_P^*, N, 1/Z_{Pg}, \sigma_g) f_{DMA}(Z_P^*, \eta, Z_P, \sigma_{g,DMA}) dZ_P^*\,, \qquad (7.7)$$

$$N_1(Z_P) = \frac{\eta N^*}{\sqrt{2\pi}\sqrt{\ln^2\sigma_g + \ln^2\sigma_{g,DMA}}}\exp\left(-\frac{1}{2}\left(\frac{\left(\ln(1/Z_P)-\ln(1/Z_{Pg})\right)^2}{\ln^2\sigma_g+\ln^2\sigma_{g,DMA}}\right)\right), \qquad (7.8)$$

$$N_1(Z_P) = f_{LN}\left(1/Z_P, N^*, 1/Z_{Pg}, \exp\left(\sqrt{\ln^2\sigma_g + \ln^2\sigma_{g,DMA}}\right)\right). \qquad (7.9)$$

Using this formula, the actual parameters of the mobility distribution can be determined provided that $\sigma_{g,DMA}$ is known. The initial calibration (chapter 2) of the nano-RDMA did not extend into this mobility range, but the approximate value of $\sigma_{g,DMA}$ can be calculated based on the instrument calibration factor (G = 17.3).[4] The extrapolated values of $\sigma_{g,DMA}$ are much smaller than the breadth of the measured mobility distribution. Therefore, the measured mobility distribution is approximately correct provided that the instrument resolution can be extrapolated.

The size distributions measured using the first nano-RDMA can be transmitted to the second nano-RDMA and measured for mobility distribution, as shown in figure 7.3. The mobility distributions represent the convolution of three log-normal distributions:

$$N_2(Z_P) = \int_0^\infty f_{LN}(1/Z_P^*, N, 1/Z_{Pg}, \sigma_g) f_{DMA}(Z_P^*, \eta_1, Z_{PDMA1}, \sigma_{g,DMA1}) f_{DMA}(Z_P^*, \eta_2, Z_P, \sigma_{g,DMA2}) dZ_P^*, \tag{7.10}$$

$$N_2(Z_P) = \frac{\eta_1\eta_2 N^\#}{\sqrt{2\pi}\sqrt{\ln^2\sigma_{DMA2} + \frac{\ln^2\sigma_g \ln^2\sigma_{DMA1}}{\ln^2\sigma_g + \ln^2\sigma_{DMA1}}}} \exp\left(-\frac{1}{2}\left(\frac{\left(\ln(Z_P) - \frac{\left(\ln Z_{Pg}\ln^2\sigma_{DMA1} + \ln Z_{DMA1}\ln^2\sigma_g\right)}{\ln^2\sigma_g + \ln^2\sigma_{DMA1}}\right)^2}{\ln^2\sigma_{DMA2} + \frac{\ln^2\sigma_g \ln^2\sigma_{DMA1}}{\ln^2\sigma_g + \ln^2\sigma_{DMA1}}}\right)\right), \tag{7.11}$$

$$N_2(Z_P) = f_{LN}\left(Z_P, \eta_1\eta_2 N^\#, \frac{\left(\ln Z_{Pg}\ln^2\sigma_{DMA1} + \ln Z_{DMA1}\ln^2\sigma_g\right)}{\ln^2\sigma_g + \ln^2\sigma_{DMA1}}, \exp\left(\sqrt{\ln^2\sigma_{DMA2} + \frac{\ln^2\sigma_g \ln^2\sigma_{DMA1}}{\ln^2\sigma_g + \ln^2\sigma_{DMA1}}}\right)\right), \tag{7.12}$$

that is also found to be a lognormal distribution. In the limit of $\ln^2\sigma_g >> \ln^2\sigma_{DMA1}$ with $Z_{pg} \approx Z_{DMA1}$, this expression becomes

$$N_2(Z_P) = f_{LN}\left(Z_P, \eta_1\eta_2 N^\#, \ln Z_{DMA1}, \exp\left(\sqrt{\ln^2\sigma_{DMA2} + \ln^2\sigma_{DMA1}}\right)\right). \tag{7.13}$$

The mobility distributions are narrower than the initial mobility distribution, and contain fewer particles. The decrease in number of particles is expected since particle loss occurs in the nano-RDMA, and can be accounted for with the parameter η_2. Particle deposition can occur in a few locations due to diffusion to any of the walls or to electrophoresis in the aerosol inlet region.

The distributions measured in the second nano-RDMA are better visualized after normalizing the data, shown in figure 7.4 for silane concentrations of 1 to 4 ppm. The mobility is normalized with respect to mobility selected in the first DMA and the current is normalized with the current measured in the first nano-RDMA. The first observation is that all of the distributions are shifted to lower mobilities (i.e., larger particle sizes). The shift is captured by a parameter $\delta = Z_{DMA2}/Z_{DMA1}$, and is plotted in figure 7.5. It increases with voltage and levels off at a value of 0.96. This shift has been observed in many TDMA measurements, but is not well understood.[*11*]

The second observation from the normalized data concerns the transmission, and is shown in figure 7.6 for each of the concentrations tested. The fraction transmitted increased with voltage from 0.1 for the low voltage range tested to a value of 0.2 for the high voltage range. The increase in transmission with voltage most likely corresponds to less deposition due to diffusion since smaller particles (transmitted at lower voltages) will diffuse faster than larger particles.

The transmission was approximately constant for the higher voltage range and could correspond to the limiting transmission for this flow rate ratio. Electrophoretic deposition in the aerosol inlet extension region (see chapter 2 for description) most likely

reduces the transmission through the device. If higher transmissions were desired, the aerosol flow rate could be increased or the inlet extension could be lengthened.

The final observation from the normalized data is the resolution, and is shown in figure 7.7. The resolution was determined from fitting the measured distribution using a lognormal function. Assuming the resolution of the first and second nano-RDMA was approximately equal and using the relation found in equation (7.13), the resolution was determined as a function of voltage. The resolution increases with voltage to a maximum of ~7.5. The increase in resolution was expected, but the resolution is lower than expected and observed previously (chapter 2). The resolution measured using molecular ions at a voltage of ~150 V was approximately 7. The resolution found using the microplasma at this voltage was ~4.2.

The lower-than-expected resolution indicates that the microplasma is not an ideal calibration source in this configuration. A number of reasons could be responsible for the low resolution, including aspherical particles and space-charge distortion in the DMA.[*12-14*] Aspherical particles will be transmitted over a larger range of voltages as they are transmitted with a random orientation through the nano-RDMA. Since a DMA measures the average mobility in an electric field, the random orientation will affect the average drag force and consequently the range of voltages over which the particle is transmitted.

Broadening due to space-charge distortion of the electric field is the second possibility. Space-charge effects were determined theoretically to be important for values of $n_o Z\tau$ larger than 22,000 V^{-1} cm^{-1},[*12*] where n_o is the number concentration at the inlet, Z is the electrophoretic mobility, and τ is the residence time in the device. Given that the

residence time inside of the nano-RDMA (τ) is approximately 25 ms, the measured value of n_o is approximately 10^6 cm^{-3}, and Z is approximately 0.5 cm^2 V^{-1} s^{-1}, the value calculated for the instrument is 12,500 V^{-1} cm^{-1}. Depending upon where the particle losses in the instrument occur, the measured value of n_o could be higher, resulting in space-charge distortion that would cause broadening of the mobility distribution. The calculated values do not indicate space-charge distortion, but the mobility distribution behaves as would be expected for such an effect (i.e., the mobility measured in the second DMA is higher than the mobility set with the first DMA and the distribution is broadened). The effect of space-charge distortion would not be expected in the second nano-RDMA because the lower concentration would limit these effects and not affect the measured size distribution.

7.4. Summary

A microplasma source was demonstrated to operate stably producing a high concentration of nanoparticles over a broad mobility range. The microplasma most likely could not be used as a calibration standard to use in the TDMA since the measured mobility distributions did not indicate a resolution as high as previously measured using molecular ions.

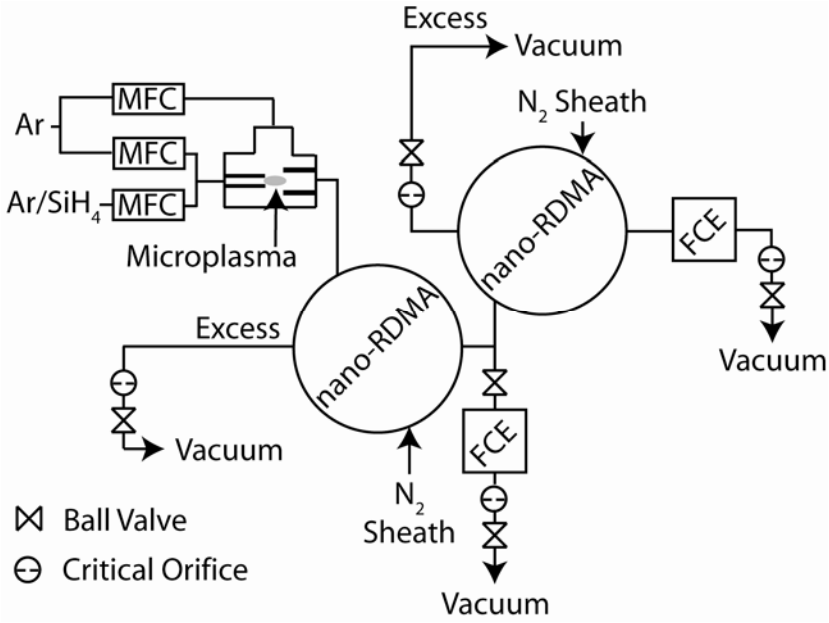

Figure 7.1 Schematic of Tandem DMA.

Schematic of the microplasma and tandem differential mobility analyzer arrangement used to calibrate the nano-RDMA.

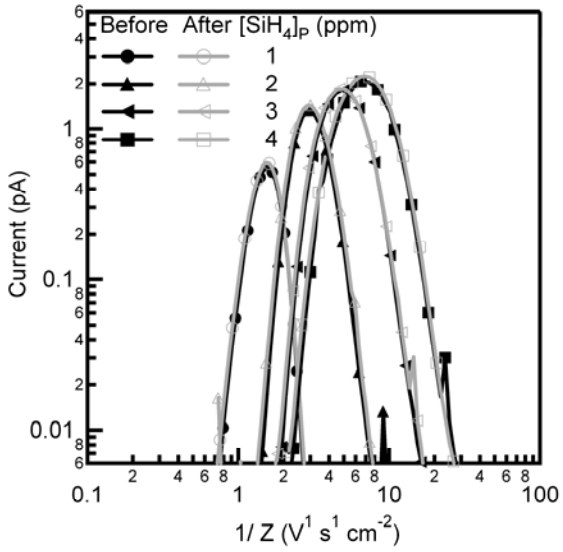

Figure 7.2. Mobility Distribution from First nano-RDMA.

Mobility distribution measured with the first nano-RDMA before and after the TDMA measurement. The microplasma was operated with a current of 7.5 mA and a total flow rate of 600 sccm.

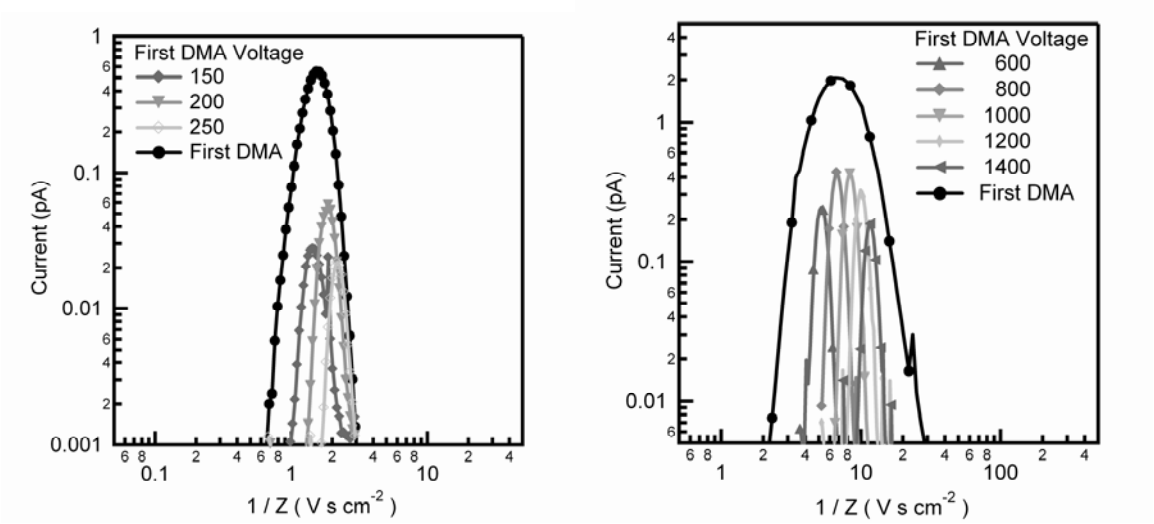

Figure 7.3. TDMA Mobility Distributions.

TDMA mobility distributions measured from the microplasma using silane concentrations of 1 (left) and 4 (right) ppm. The mobility distributions are labeled with the voltage applied to the first nano-RDMA. The mobility distribution from the first nano-RDMA (black circles) is indicated for reference.

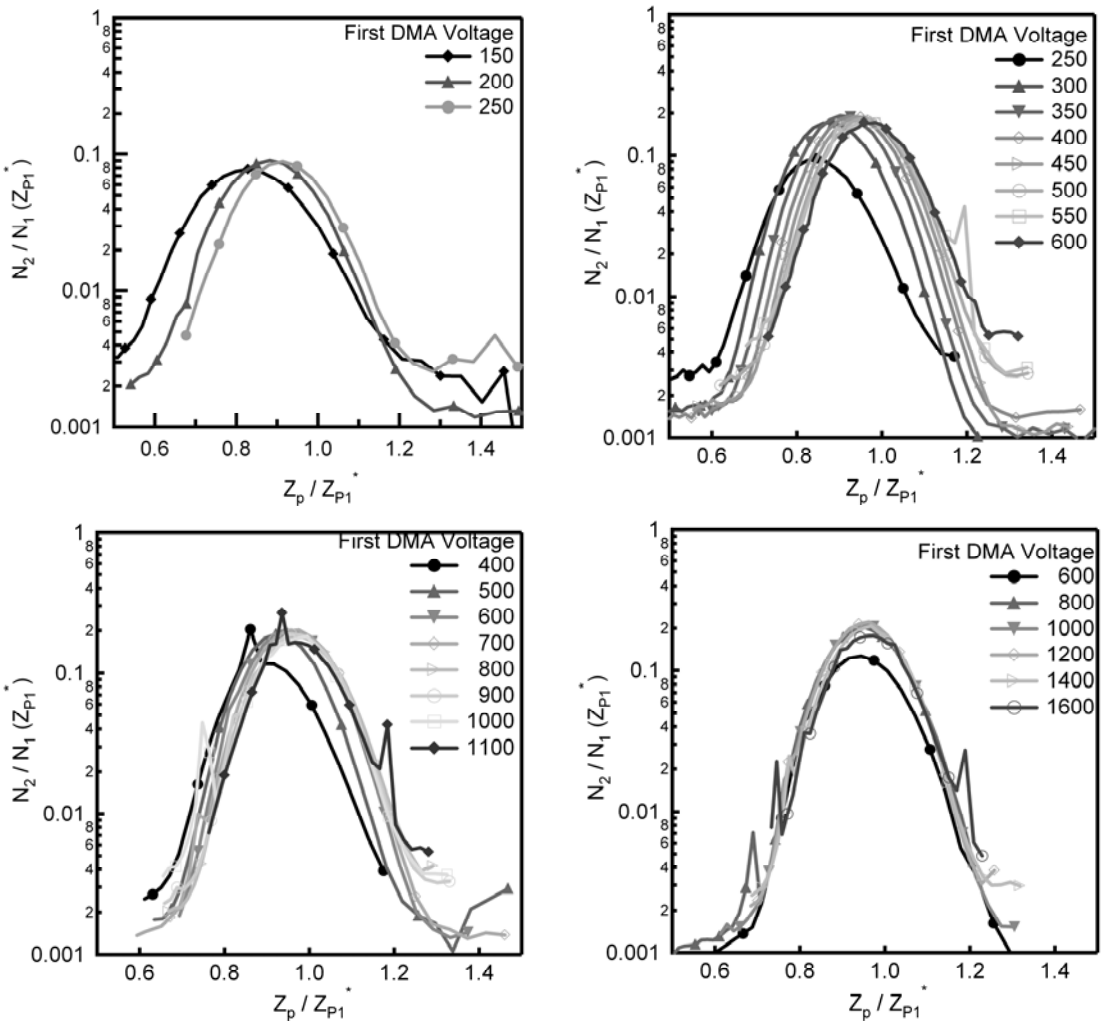

Figure 7.4. Normalized TDMA Mobility Distributions.

Normalized TDMA mobility distributions using silane concentrations of 1 (top left), 2 (top right), 3 (bottom left), and 4 (bottom right) ppm in the microplasma. The concentration data are normalized by the concentration measured with the first nano-RDMA at the set mobility. The mobility data are normalized by the mobility set on the first nano-RDMA.

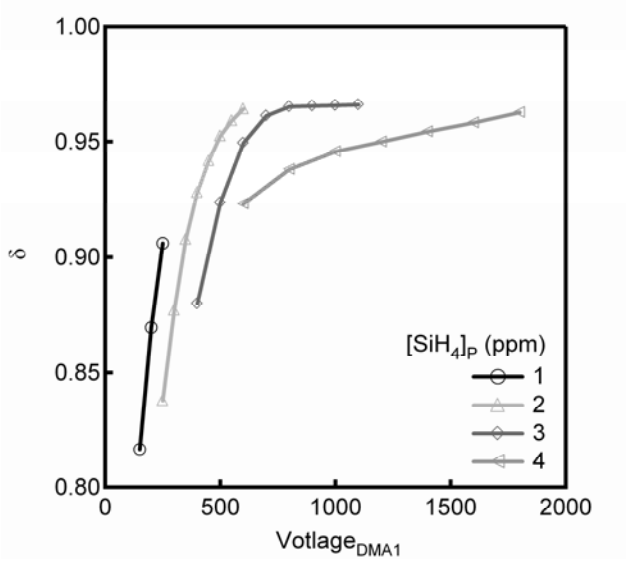

Figure 7.5. Shift of TDMA Mobility Distribution.

The measured shift in the mobility distribution from the expected mobility ($\delta = Z_{DMA2}/Z_{DMA1}$) as a function of voltage.

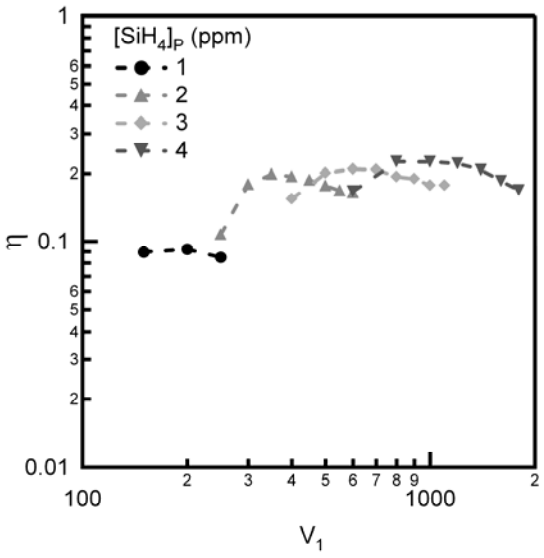

Figure 7.6. Transmission of the nano-RDMA.

The measured transmission (η) of the second nano-RDMA as a function of voltage.

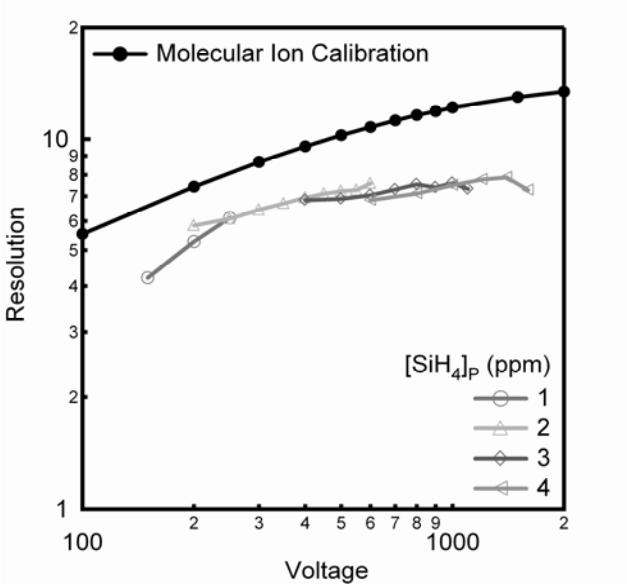

Figure 7.7. Resolution Measured with the Tandem DMA.

The measured resolution from the nano-RDMA as a function of voltage. The resolution measured with the molecular ion is extrapolated into this region.

Table 7.1. Fitting Parameters of First nano-RDMA Mobility Distributions

The fitting parameters of a log-normal distribution for the mobility distributions measured with the first nano-RDMA.

$[SiH_4]$ (ppm)	*Current* (pA)	Z^{-1} (V s cm^{-2})	*ln* σ -	σ_g
1	0.295 ± 0.013	1.526 ± 0.009	0.204 ± 0.002	1.23
2	0.855 ± 0.036	2.995 ± 0.013	0.245 ± 0.006	1.28
3	1.456 ± 0.055	4.907 ± 0.030	0.321 ± 0.006	1.38
4	1.961 ± 0.098	6.884 ± 0.021	0.393 ± 0.003	1.44

References

1. P. Winkler, G. Steiner, A. Vrtala, H. Vehkamaki, M. Noppel, K. Lehtinen, G. Reischl, P. Wagner, and M. Kulmala, *Science,* **319**, 1374, 2008.
2. J. Heintzenberg, B. Wehner, and W. Birmili, *Tellus,* **59**, 273, 2007.
3. J. Seinfeld, and S. Pandis, *Atmospheric chemistry and physics*. (John Wiley and Sons, Inc., New York, 1998).
4. N. Brunelli, R. Flagan, and K. Giapis, *Aerosol Science and Technology,* **43**, 53, 2008.
5. W. Birmili, F. Stratmann, A. Wiedensohler, D. Covert, L. Russell, and O. Berg, *Aerosol Science and Technology,* **27**, 215, 1997.
6. S. Ude, and J. Fernandez de la Mora, *Journal of Aerosol Science,* **36**, 1224, 2005.
7. R. Sankaran, D. Holunga, R. Flagan, and K. Giapis, *Nano Letters,* **5**, 537, 2005.
8. L. Kiss, J. Söderlund, G. Niklasson, and C. Granqvist, *Nanostructured Materials,* **12**, 327, 1999.
9. M. Stolzenburg, and P. McMurry, *Aerosol Science and Technology,* **42**, 421, 2008.
10. M. Stolzenburg, University of Minnesota (1988).
11. Y. Kousaka, K. Okuyama, M. Adachi, and T. Mimura, *Journal of Chemical Engineering of Japan,* **19**, 401, 1986.
12. M. Alonso, F. Alguacil, and Y. Kousaka, *Journal of Aerosol Science,* **31**, 233, 2000.
13. M. Alonso, and Y. Kousaka, *Journal of Aerosol Science,* **27**, 1201, 1996.

14. R. P. Camata, H. A. Atwater, and R. C. Flagan, *Journal of Aerosol Science,* **32**, 583, 2001.